

Integrated Communication and Imaging: Design, Analysis, and Performances of COSMIC Waveforms

Marco Manzoni*, Francesco Linsalata*, Maurizio Magarini, and Stefano Tebaldini
 Department of Electronics Information and Bioengineering, Politecnico di Milano, Milan, Italy
 (correspondence: marco.manzoni@polimi.it, francesco.linsalata@polimi.it)

Abstract—This paper proposes a novel waveform design approach named COSMIC (Connectivity-Oriented Sensing Method for Imaging and Communication). The generation of radio images of the environment is enabled by imposing an extended orthogonality condition among waveforms. In contrast to traditional time, frequency, or space multiplexing systems, COSMIC achieves orthogonality through algebraic precoding of the transmitted waveforms from all antennas. Furthermore, by leveraging the degrees of freedom inherent in the assumption that the imaging field of view is significantly smaller than the length of the transmitted signals, the resulting waveforms are designed to convey communication symbols without impeding the sensing operations. We analytically demonstrate that the efficiency of imaging and communication sub-systems can be tuned according to the specific use case requirements. Simulation results indicate that COSMIC waveforms facilitate accurate environmental imaging while preserving near-optimal communication performance in terms of error rate and capacity.

Index Terms—6G, Integrated Communication and Imaging, Waveform Design, Coding, Zero-Correlation

I. INTRODUCTION

Wireless communication and radar have traditionally been approached as two independent systems, utilizing distinct hardware, waveforms, and spectral components, seldom converging, and with different objectives: information transport and environment sensing. In the current vision of the next cellular networks, namely the sixth generation (6G), sensing is perceived as an add-on feature supporting communication, which remains the primary function. This new vision is based on the paradigm of seamlessly integrating radar functionalities into communication systems [1]–[3].

Integrating radar operations seamlessly without disrupting information transmission poses a significant challenge for such systems. Several works have focused on implementing a combined radar and communication system by transmitting a single waveform that is capable of jointly transmitting information to a target and retrieving sensing information about the target itself [1], [2], [4]–[9].

The most common approaches limit the radar capabilities to estimate range, angle, and Doppler. This is typically associated with the traditional radar concept that aims at obtaining basic information about some detected targets. These parameters are

essential for understanding a target’s location, velocity, and direction within the radar’s field of view [10]. However, most radar applications extend beyond these estimations. Indeed, radar’s primary objective is imaging. Radar imaging means forming detailed electromagnetic images of an entire scene of interest, allowing for a complete understanding and characterization of the environment composed of a continuous distribution of targets in the radar field of view.

Imaging applied in spatially extended scattering scenarios requires that the waveforms transmitted by the radar or Rad-Com antennas are *perfectly orthogonal* for any arbitrary shift between different transmitted signals [11]. Nevertheless, the field of view is limited in most applications. For example, the maximum practical range of automotive radars (radar-to-target distance) is a few hundred meters. This condition allows for relaxation of the orthogonality requirement between the transmitted waveforms since it is no longer mandatory that they are orthogonal for *any* shift, but only for those shifts that the targets in the scene could induce. This condition introduces some degrees of freedom that this work aims to exploit. In particular, we can encode information inside the waveforms, transmitting communication symbols while simultaneously performing the imaging. In this context, we propose a waveform design method for simultaneous imaging and information transmission. Furthermore, we model its processing chain along with the description of the procedure adopted at the communication receiver to decode the information and at the sensing receiver to generate an image of the environment. The efficiency of both communication and sensing can be tuned according to specific needs, privileging one or the other system.

Paper Contributions The main contributions of this work can be summarized as follows.

- Development of a novel waveform design method named COSMIC (Connectivity-Oriented Sensing Method for Imaging and Communication). COSMIC waveforms are engineered to convey an effective integration of radar imaging and communication functionalities within the same system. COSMIC is based on the degrees of freedom provided by the intuition that the imaging field of view is significantly smaller than the length of the transmitted signals, enabling information transmission.
- Demonstrates that the orthogonality among COSMIC waveforms is achieved without relying on time or frequency separation but using a precoding operation obtained by an algebraic approach.

This work was partially supported by the European Union under the Italian National Recovery and Resilience Plan (NRRP) of NextGenerationEU, partnership on “Telecommunications of the Future” (PE00000001 - program “RESTART”) CUP: D43C22003080001.

*These authors equally contributed to this research

- Provide a detailed description of the required processing procedure for waveform generation. The workflow employed on the communication and imaging receivers is also detailed.
- Discuss the flexibility of COSMIC in optimizing the imaging and communication systems. The proposed design can arbitrarily tune the efficiency of the imaging and communication sub-systems, prioritizing one over the other based on the scenario, the amount of information to be transmitted, and the desired imaging resolution.
- Highlight the COSMIC waveforms' capability to enable accurate environmental imaging and detect faint targets while maintaining an acceptable performance at the communication receiver without any significant processing.

Paper Organization The rest of the paper is organized as follows: Section II explores the state-of-the-art in the field of integrated communication and sensing, highlighting the performances and limitations of each method. Section III is the main one and details the entire algorithm for generating the waveforms. In contrast, Section IV describes the processing at the imaging receiver to create the radio image of the environment and the one at the communication receiver to decode symbols. Section V explains how to tune the efficiency of the two sub-systems, while Section VI provides the simulation results and shows the performances. Finally, Section VII draws the conclusion.

II. RELATED WORKS

The following subsections provide an overview of the state-of-the-art solutions of sensing-centric and communication-centric solutions.

A. Communicating through Radar Waveforms

The implementation of communication within radar systems necessitates the use of either pulsed or continuous-wave radar signals. Consequently, embedding information with minimal interference on radar operation emerges as one of the primary challenges [12].

Embedding a communication signal into radar emission for dual functionality was discussed in [13]. In this approach, the radar waveform is chosen on a pulse-to-pulse basis from a bank of waveforms, each representing a communication symbol. The communication receiver decodes the embedded information by identifying the transmitted waveform.

In [14], the authors propose the design of integrated radar and communication systems that utilize weighted pulse trains with the values of the Oppermann sequences serving as complex-valued weights. Such an approach naturally co-exists with communication code division multiplexing solutions. However, phase modulation can lead to waveform alteration and, consequently, energy leakage outside of the assigned bandwidth.

One particularly intriguing technique for embedding information in radar signals is Index Modulation (IM). Such a design allows for embedding information into various combinations of radar signals' parameters across one or more domains, including space, time, frequency, and code [15]–[18].

IM-based approach can be implemented in most of the current radar system, however the communication capacity is limited by the slot time coding of the radar pulse repetition frequency (PRF). Thus, IM waveforms require a trade-off between data rate and robustness and tend to be more complex to design and implement than traditional waveforms.

In spatial embedding, the information bits are modulated through the side-lobes of radar beams-patterns [12]. However, the performance is sensitive to the array calibration and multipath interference.

The Pulse Position Modulation (PPM) encodes data by varying the position of radar pulses within the waveform, allowing the transmission of digital information without significantly impacting radar performance [19].

Radar systems, known for their extensive operational range spanning hundreds of kilometers, offer a significant advantage for implementing very long-range communication with substantially lower latency. However, the communication capacity achievable in such systems is often restricted due to inherent limitations in radar waveform design, whose primary aim, sensing the environment, is different.

B. Sensing through Communication Waveform

In communication-centric approaches, radar sensing is incorporated into existing communication systems as a secondary function. The paper in [20] addresses the sensitivity of sensing applications using Constant-Amplitude Zero Auto-Correlation (CAZAC) sequences to severe Doppler shifts, especially in high-mobility scenarios. It introduces a parameter design approach to enhance the resilience of CAZAC sequences to Doppler effects. However, in such a design, CAZAC sequences have been used by the communication infrastructure only for sensing the environment without carrying information.

Cyclic Prefix Orthogonal Frequency Division Multiplexing (CP-OFDM) has emerged as a favorable option for both communication and sensing purposes [21]. However, the high peak average power ratio of CP-OFDM can present challenges, particularly in radar applications where power efficiency holds significant importance.

As an alternative, the Frequency Modulated Continuous Wave (FMCW) waveform, typically employed in radar applications, has been studied for Integrated Sensing and Communication (ISAC) applications. Attempts have been undertaken to adapt the FMCW waveform for communication applications, such as employing up-chirp for communication and down-chirp for radar or introducing modulation schemes like trapezoidal frequency modulation continuous-wave [22]. However, these approaches encounter difficulties associated with limited spectral efficiency owing to the chirp-like nature of the sensing signal.

Another direction of investigation delves into single-carrier waveforms, combining the advantages of a simplified modulation scheme with interference sensing capabilities [23]. However, in single-carrier waveforms, spectrum efficiency may become a critical factor.

A common approach involves directly optimizing the time-frequency resource allocation by employing the current 5G

New Radio waveform OFDM. The OFDM for sensing purposes is widely explored in literature [24]–[39]. The authors of [27] suggest super-resolution range and velocity estimators for OFDM-based ISAC systems. The paper [29] examines a mutual information-based power optimization technique that determines the power allocation plan for ISAC systems that are radar- and communication-centric. In order to design the OFDM ISAC waveform, in [31], [32], the use of information-theoretic metrics is applied to the communication and sensing channels. The authors of [35] address the practical concerns of 5G OFDM for delay/Doppler estimation, including processing chain complexity and self-interference. They provide experimental results to show that OFDM range/Doppler imaging is feasible. The authors of [39] make another noteworthy contribution to waveform design through optimized OFDM by determining the best timing, frequency, and power resource allocation for several targets' delays and Doppler Cramér–Rao bounds. The authors draw attention to the issue of the resulting waveform's ambiguity function, whose sidelobes may conceal weak targets that are unknown at the time of optimization.

Orthogonal Time Frequency Space (OTFS) has emerged as a potential candidate waveform for sensing and communication [40]–[42]. OTFS-based ISAC systems offer special features thanks to their robustness against delays and Doppler frequency shifts, as well as the ability to engage directly with channel replies in a unified delay-Doppler domain. However, considerable adjustments and standardization work would be needed to include OTFS in the current 5G NR system. A dual domain waveform design, which exploits the OFDM and OTFS principles, has been proposed in [43], [44]. The works demonstrate that a wideband and low-power sensing signal can be superimposed to standard communication waveform for mono-static range and Doppler estimation.

Affine frequency division multiplexing (AFDM) has been proposed waveform that achieves optimal diversity gain in high mobility scenarios and has appealing properties in high-frequency communication. In [45], an AFDM-based ISAC system is presented in order to identify all delay and Doppler components associated with the propagation medium.

The work [46] analyzes the sensing and communication performance relying on random signaling in a multi-antenna system. They investigate a data-dependent precoding scheme to optimize the performance in sensing-only scenarios.

In all the aforementioned research works, the sensing accuracy on delay/range and Doppler/velocity estimation is limited by the allocated bandwidth and signal burst duration, respectively. None of the proposed solutions have put forward a processing chain dedicated to designing waveforms suitable for simultaneous radar imaging of a scene and information transmission. The only work that proposes a joint communication and SAR imaging (JCASAR) system using CP-OFDM for simultaneous target profile reconstruction and communication is [47]. The authors optimize waveform design by minimizing the mean squared error of the least squares estimator and develop power allocation strategies for Gaussian-distributed ISAC signals to balance communication and imaging performance. However, the system requires running an optimization problem based on the performance targets of JCASAR.

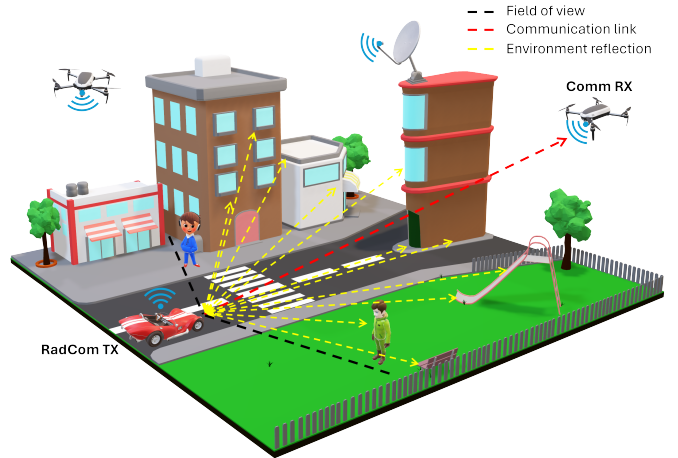


Fig. 1: Pictorial representation of the extended scattering scenario. One entity (in this case the red vehicle) wants to transmit information and, at the same time, wants to form a radio image of the scenario.

III. WAVEFORM DESIGN

The steps for designing the COSMIC waveforms and the processing for radar and communication receivers are explained in this section.

We consider a RadCom device that is a Multiple-Input Multiple-Output (MIMO) system, transmitting information symbols to other connected entities while simultaneously performing radar functions. The RadCom MIMO device has N transmitting antennas and M receiving antennas to record the echoes scattered by the scattering points in the scene. Each point induces a different delay in the signal proportional to the two-way travel time from the RadCom device to the point and back, resulting in echoes arriving at the receiver with different delays. Each transmitting antenna sends a waveform with bandwidth B and duration T_p . The N waveforms are transmitted simultaneously, sharing the same portion of the spectrum. The communication receiver simultaneously receives the superimposed N transmitted waveforms and decodes the information.

Let us define the set of transmitted waveforms in continuous time domain t as

$$\mathcal{S} = \{s_1(t), s_2(t), \dots, s_N(t)\}, \quad (1)$$

where each waveform $s_n(t)$ is transmitted by the n th Tx antenna with $n = 1, \dots, N$. The coherent superposition of all the delayed waveforms is recorded at the co-located receiver. By defining the transmitted signal $s(t)$ as

$$s(t) = \sum_{n=1}^N s_n(t), \quad (2)$$

the corresponding received echo can be written as $s(t - \tau)$, where τ is the total travel time, i.e., from the transmitter to a generic target and from the target to the receiver.

A. Orthogonality condition for extended scattering scenario

The transmitted waveforms in \mathcal{S} must be opportunely designed such that after the range compression¹ at the imaging receiver, the single contributions of the N transmitted signals can perfectly be separated at each of the M receiving antennas. The condition for a perfect separation of the scattered waveforms from a single point target is

$$\int_{-\infty}^{+\infty} s_n^*(\eta) s_m(\eta) d\eta = 0 \quad \forall \quad m \neq n. \quad (3)$$

The condition in (3) is equivalent to enforcing the spatial covariance matrix of the transmitted waveforms to be the identity matrix as in [48].

It is worth stating that in case of an extended scattering scenario, where an infinite number of infinitesimal scatterers are distributed at many different distances from the radar, it is *not sufficient* to impose the condition in (3). Indeed, the condition in (3) does not allow for perfect signal separation, which is necessary for imaging purposes [11]. This concept is demonstrated in Appendix A.

The orthogonality condition must be satisfied for *all the possible differences of delays* induced by the targets in the scene. Taking the automotive scenario in Figure 1 as a reference, the maximum difference of distance is, say, 100 meters; thus, the zero correlation interval should be imposed for 100 meters. The extended scattering orthogonality condition can be written as

$$r_{nm}(t) = s_n^*(-t) * s_m(t) = \int_{-\infty}^{+\infty} s_n^*(\eta) s_m(\eta + t) d\eta = 0, \quad \forall \quad m \neq n, \quad 0 \leq t \leq \tau_s. \quad (4)$$

where τ_s is the maximum two-way travel time of the waveforms. Equation (4) implies that cross-correlation must be strictly zero *only within a range of delays* that depends on the maximum distance traveled by the signal in the whole path from the transmitter to the receiver. As an example, if the maximum range for a target is $r_{\max}=100$ m and TX/RX are co-located, the maximum delay that the signal experiences is $\tau_s = 2r_{\max}/c = 0.67\mu s$, where c is the speed of the light.

Thus, the cross-correlation of the waveforms must be zero between 0 and τ_s , while no constraints are enforced in the region of $t < 0$ and $t > \tau_s$ since there the orthogonality is not required.

The result of a simple simulation of an extended scattering scenario is represented in Fig. 2. The simulated scene comprises two highly reflective targets placed close to each other and 100 loosely reflecting scatterers randomly placed in the field of view at different distances. The scene is illuminated by 101 antennas, transmitting either a COSMIC waveform or a waveform that is strictly orthogonal only for zero mutual shift. The signal is range-compressed at the receiver, and the output is averaged for all the waveforms, leading to the result in Fig. 2. It is easy to see how, in the case of zero-shift orthogonal

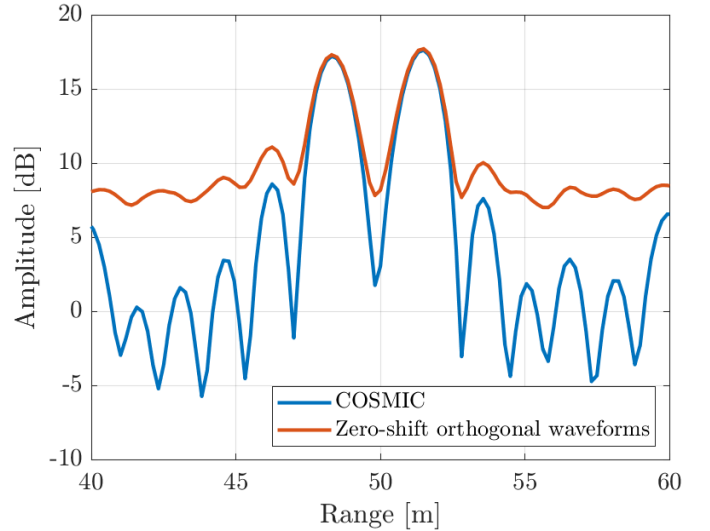


Fig. 2: Average range compressed data. The scene, composed of two highly reflective targets and 100 loosely reflective ones, is illuminated by 101 waveforms simultaneously. The simulation is carried out with COSMIC waveforms and waveforms that are strictly orthogonal only for mutual shifts equal to zero as in (3).

waveforms, the noise floor is much higher since the energy related to all the elementary scatterers adds up, worsening the system's performance. Finally, with an even higher number of scatterers and/or antennas, the highly reflective targets can be entirely hidden by the MIMO noise, which is the noise introduced by the fact that two waveforms are not orthogonal. After the range compression, the region with positive delays is equal to the signal length T_p , with $T_p > \tau_s$. A typical value for T_p for automotive applications is $50\mu s$ [49], corresponding to a signal length of 7.5 km. On the other hand, the interval in which we must enforce perfect orthogonality is, for example, 100 m, an order of magnitude shorter than the pulse length. Therefore, we can use this remaining and unused area to inject information into the transmitted waveforms. This demonstrates one of the main features of the COSMIC design and paper contribution.

B. COSMIC design

By denoting a sampling frequency f_s in Hz, the sampling interval is $T_s = 1/f_s$ and the discrete-time signal is $s_n(kT_s) = s_n$ with $k = 0, 1, \dots, K-1$, where K is the total number of transmitted symbols. We assume that all the transmitting antennas send a signal that contains informative data for a communication receiver. This assumption can be relaxed to improve sensing efficiency as explained in Sec. V.

With reference to Fig. 3, the n th signal is written as a linear combination of orthogonal basis as

$$s_n = C_n \alpha_n, \quad (5)$$

where the vector $\alpha_n \in \mathbb{C}^{K_s \times 1}$ encodes the information and

¹Range compression and matched filtering are two different jargon used by the radar community and the communication community to indicate the filtering operation that maximizes the SNR at the receiver.

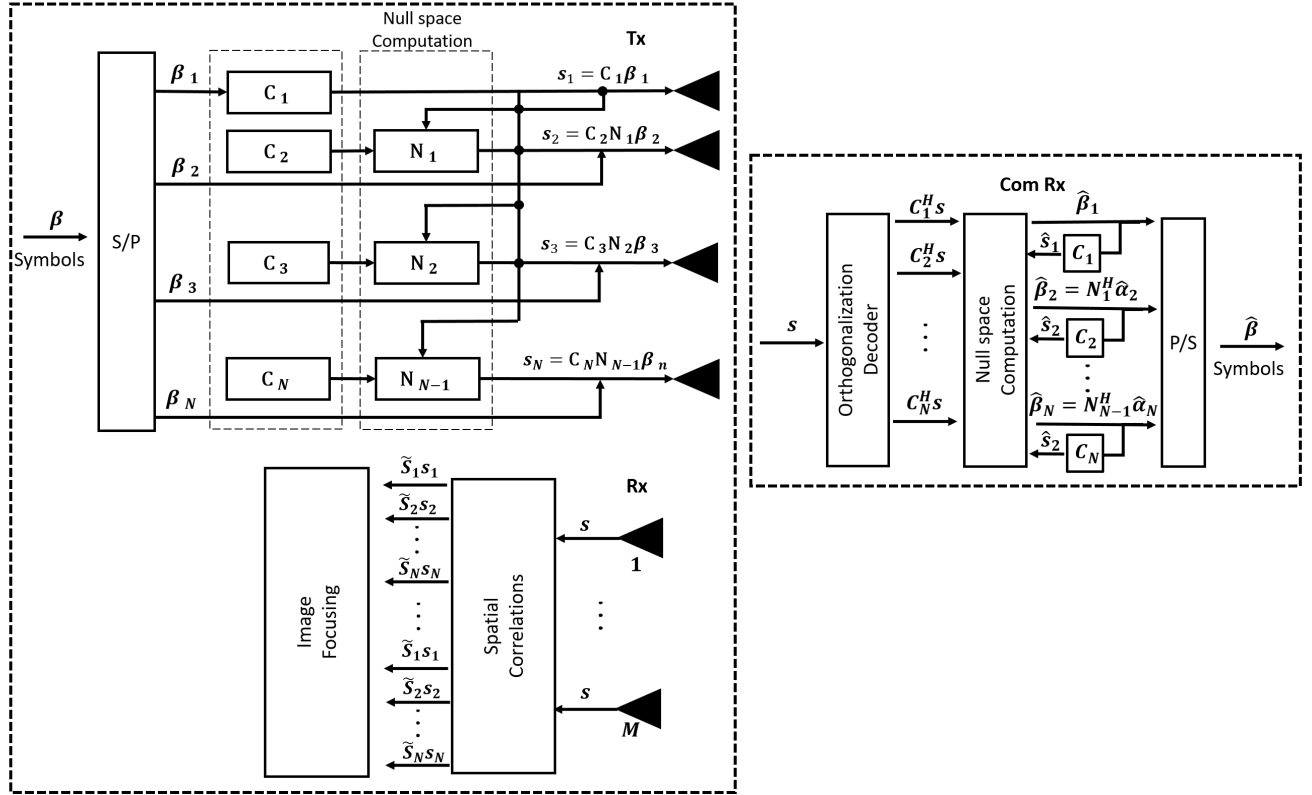


Fig. 3: COSMIC waveforms system model. The RadCom has N transmitting antennas and M receiving ones. The communication receiver simultaneously receives the superimposition of the transmitted waveform and decodes the information.

$C_n \in \mathbb{C}^{K \times K_s}$ is an orthogonal matrix such that

$$\begin{cases} C_n^H C_n = \mathbf{I} \\ C_m^H C_n = \mathbf{0}, \quad \forall m \neq n \end{cases} \quad (6)$$

where the superscript H indicates the Hermitian, \mathbf{I} is the identity matrix, and $\mathbf{0}$ is the zero matrix. The matrices C_n , refers as *keys*, encode/decode the information into/from the waveforms. The number of columns of C_n is lower or equal to the number of rows ($K_s \leq K$). These keys can be straightforwardly derived from a *master key* C . In particular, the C is a $K \times K$ orthogonal matrix whose columns are the ordered left-eigenvectors of a random matrix with dimension $K \times K$. Each matrix C_n is constructed by taking a pre-defined number of columns of C as detailed in Section V.

In the following, we detail the generation of the first three transmitted signals s_1 , s_2 , and s_3 to facilitate the main concepts behind the COSMIC waveforms construction.

As shown in Fig. 3 for the first waveform s_1 , the vector α_1 is already informative, and it contains K_s complex constellation symbols. The key C_1 projects the information into the signal space. For example, if by assuming a $50 \mu\text{s}$ signal sampled with $f_s = 300 \text{ MHz}$, it has a length of $K = 15000$ samples. With three transmitting antennas and assigning the same size keys to the antennas ($K_s = 5000$), the first waveform carries K_s communication symbols.

The second waveform s_2 is designed not only as a linear combination of vectors C_2 to ensure orthogonality to C_1 as

in (6), but also sensing-wise orthogonal as in (4). The cross-correlation (4) can be written as

$$r_{12} = \mathbf{S}_1 s_2, \quad (7)$$

where $r_{12} \in \mathbb{C}^{(2K-1) \times 1}$, $s_2 \in \mathbb{C}^{K \times 1}$ is the unknown signal, and $\mathbf{S}_1 \in \mathbb{C}^{(2K-1) \times K}$ is the cross-correlation matrix that is a convolution matrix with the time-reversed and complex conjugate entries of s_1 . It can be constructed as

$$\mathbf{S}_1 = \begin{bmatrix} s_1^*(K-1) & 0 & \dots & 0 \\ s_1^*(K-2) & s_1^*(K-1) & \dots & 0 \\ \vdots & s_1^*(K-2) & \dots & 0 \\ s_1^*(0) & \vdots & \dots & 0 \\ 0 & s_1^*(0) & \dots & s_1^*(K-1) \\ \vdots & 0 & \dots & \vdots \\ 0 & \vdots & \dots & s_1^*(1) \\ 0 & 0 & \dots & s_1^*(0) \end{bmatrix}. \quad (8)$$

In (4), the cross-correlation needs to be zero only within a relevant time interval of length τ_s centered around zero, not for all the $2K-1$ samples of the auto-correlation. By calculating the cross-correlation only within this set of possible delays, we effectively reduce the number of rows required in the matrix \mathbf{S}_1 (denoted as $K_z < K$). The discrete-time version of (4) is then

$$\tilde{\mathbf{S}}_1 s_2 = \mathbf{0}, \quad (9)$$

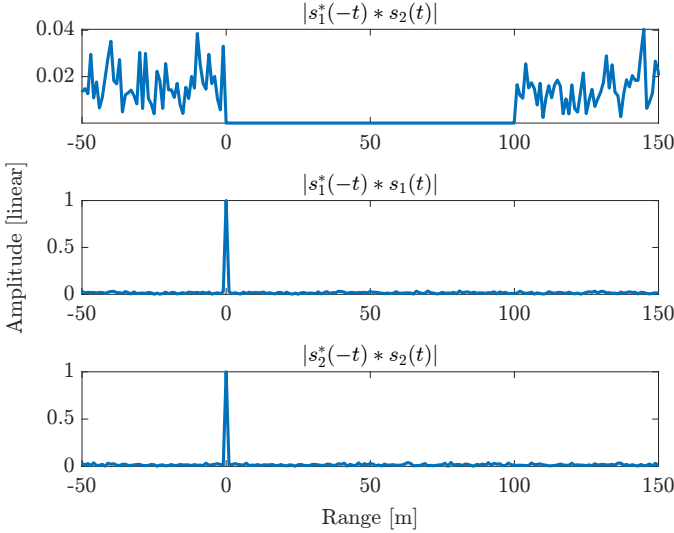


Fig. 4: (Top) Cross-correlation between the signals s_1 and s_2 . The signals are generated to have zero correlation for a length of 100 m. (Middle) The auto-correlation of s_1 shows a distinctive peak at zero delay with low sidelobes. (Bottom) The auto-correlation of s_2 .

where $\tilde{S}_1 \in \mathbb{C}^{K_z \times K}$ is a reduced version of S_1 , whose first K_z columns are considered.

By plugging $s_2 = C_2 \alpha_2$ into (9), we get

$$\tilde{S}_1 C_2 \alpha_2 = 0 \quad (10)$$

$$W_1 \alpha_2 = 0, \quad (11)$$

where $W_1 = \tilde{S}_1 C_2 \in \mathbb{C}^{K_z \times K_s}$. The size of the second key C_2 is assumed to be K_s as for the first key. Equation (10) suggests that the vector α_2 must be searched in the *null space* of the matrix W_1 :

$$\alpha_2 \in \text{null}(W_1). \quad (12)$$

In light of this, we can define the matrix $N_1 \in \mathbb{C}^{K_s \times (K_s - K_z + 1)}$ which contains the orthonormal basis spanning the null space of W_1 . Notice that W_1 is not full-rank. N_1 can be found from the Singular Value Decomposition (SVD) of W_1 , and a linear combination of its columns can be used to generate a suitable α_2 as:

$$\alpha_2 = N_1 \beta_2 \quad (13)$$

where $\beta_2 \in \mathbb{C}^{(K_s - K_z + 1) \times 1}$ is again a vector containing informative constellation symbols. The matrix N_1 can be seen as the operator projecting (or encoding) the information into the null space of W_1 . The signal to be transmitted by the second antenna can be easily derived as $s_2 = C_2 \alpha_2$. Following the previous example, if the interval at zero correlation must be 100 m, it follows that $K_z = 200$, thus the second waveform will carry 4801 symbols. When signals s_1 and s_2 are cross-correlated, there will be a region between 0 and τ_s where the cross-correlation is zero. In contrast, the correlation can assume any arbitrary value in the other region. In Fig. 4, a simulation has been carried out, and the cross-correlation between s_1 and s_2 is depicted along with their respective

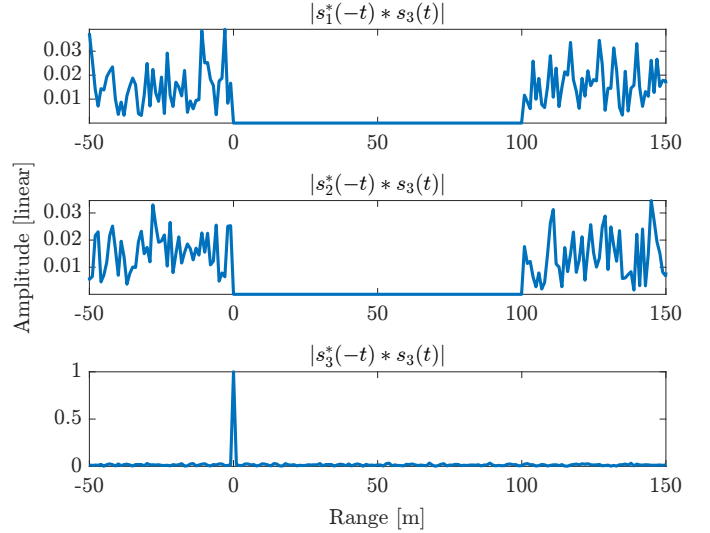


Fig. 5: (Top) Cross-correlation between the signals s_1 and s_3 . (Middle) Cross-correlation between the signals s_2 and s_3 . (Bottom) The auto-correlation of s_3 .

auto-correlations. These two signals are generated to have zero cross-correlation for 100 m while maintaining good auto-correlation properties.

The third signal s_3 must be orthogonal to both s_1 and s_2 , thus we can proceed in the same way as did so far, enforcing zero correlation for both:

$$\begin{cases} \tilde{S}_1 C_3 \alpha_3 = W_2 \alpha_3 = 0, \\ \tilde{S}_2 C_3 \alpha_3 = W_3 \alpha_3 = 0, \end{cases} \quad (14)$$

which in compact form becomes

$$\begin{bmatrix} W_2 \\ W_3 \end{bmatrix} \alpha_3 = 0. \quad (15)$$

The vector α_3 is searched in the null space of $[W_2^H, W_3^H]^T$. The size of $[W_2^H, W_3^H]^T$ is now $2K_z \times K_s$, thus the size of its null space is reduced by a factor K_z . Once again, in this particular case, the size of the third key C_3 is equal to the size of the first and the second key. The basis spanning the null space of $[W_2^H, W_3^H]^T$ are collected in the columns of $N_2 \in \mathbb{C}^{K_s \times (K_s - 2K_z + 2)}$. The vector α_3 is found as a linear combination of the columns of N_2

$$\alpha_3 = N_2 \beta_3, \quad (16)$$

where again $\beta_3 \in \mathbb{C}^{(K_s - 2K_z + 2) \times 1}$ is the vector containing the communication symbols. Then, as in the previous case, the signal s_3 can be found as $s_3 = C_3 \alpha_3$. Following again the previous example, the third waveform will carry 4602 symbols.

Figure 5 shows the cross-correlations between s_3 and the first two signals, along with its auto-correlation. The third signal is orthogonal to the other two in the usual interval, showing good auto-correlation properties.

The same reasoning in an iterative manner as in Algorithm 1 can be followed up to the point in which the size of the null-space is zero. At each iteration, the size of the null space is reduced by $K_z - 1$; thus, after approximate K_s/K_z iterations, there is no more null space to be used to find another

Algorithm 1 COSMIC waveforms generation

Require: Orthogonal matrix $C \in \mathbb{C}^{K \times K}$
Ensure: Orthogonal signals s_n for $n = 1, \dots, N$

- 1: Get $C_1 \in \mathbb{C}^{K \times K}$ from C
 - 2: Compute $s_1 = C_1 \alpha_1$, where $\alpha_1 \in \mathbb{C}^{K_s \times 1}$
 - 3: **for** $n = 2$ to N **do**
 - 4: Get $C_n \in \mathbb{C}^{K \times K}$ from C
 - 5: Compute the cross-correlation matrix S_{n-1} for s_{n-1} as (8)
 - 6: Select K_z rows from S_{n-1} to form \tilde{S}_{n-1}
 - 7: Compute $W_{n-1} = \tilde{S}_{n-1} C_n$
 - 8: Find the orthonormal basis spanning the null space of N_{n-1} of $[W_1, \dots, W_{n-1}]^T$
 - 9: Generate the communication symbols $\beta_n \in \mathbb{C}^{(K_s - n(K_z - 1)) \times 1}$
 - 10: Compute $\alpha_n = N_{n-1} \beta_n$
 - 11: Compute $s_n = C_n \alpha_n$
 - 12: **end for**
-

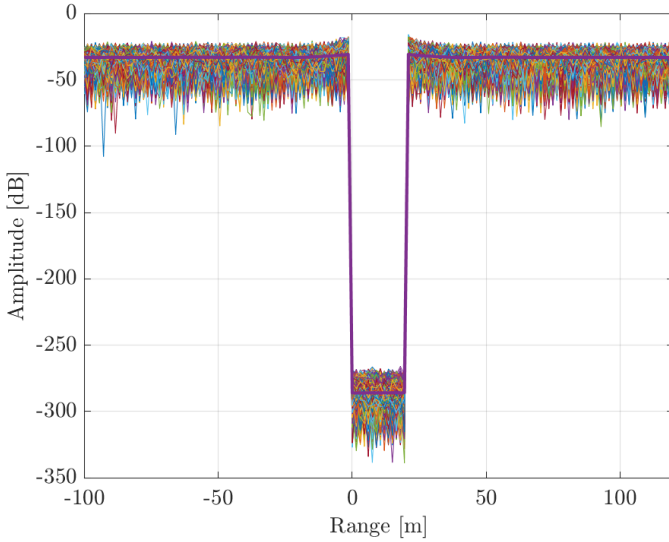


Fig. 6: All the possible cross-correlations between 101 COSMIC waveforms. The waveforms have been generated by imposing a zero-correlation length of 20 meters.

signal, and this condition sets the upper bound for the number of antennas that can be used. It is straightforward to notice that the smaller the required interval at zero correlation, the more waveforms can be generated since, at each iteration, the dimension of the null space will be reduced by a smaller quantity.

As an example, in Fig. 6, a set of 101 waveforms has been generated using the described procedure. The figure shows all the 5050 possible cross-correlations between the waveforms, while in purple the average cross-correlation. The floor of the zero correlation zone is 250 dB lower than the average correlation in the other portion of the range axis, and the lower bound is only limited by the numerical accuracy of the device.

IV. PROCESSING AT THE COMMUNICATION AND SENSING RECEIVERS

The communication receiver derives the *keys* from the *master key* and decodes the information symbols. Meanwhile, the RadCom device performs standard imaging procedures with all the received echoes to create an electromagnetic image of the environment.

At the receiver, either the communication or sensing one, the antennas record the coherent superposition of all the signals. Without loss of generality, the delays introduced by the signal propagation are neglected. In a real implementation, the delays induced by the propagation are handled as in standard OFDM concerning the communication sub-system, while they are handled as in standard array processing in the imaging sub-system. The received signal can be written as:

$$\begin{aligned} s &= s_1 + s_2 + \dots + s_N \\ &= C_1 \alpha_1 + C_2 \alpha_2 + \dots + C_N \alpha_N. \end{aligned} \quad (17)$$

The following subsections present the processing required at the communication and imaging receivers. Both processing schemes are reported in Fig. 3.

A. Communication receiver

The communication receiver is not co-located with the transmitter. The decoding procedure in the noiseless scenario is highlighted here to describe the main algebraic features of the COSMIC system. At the same time, an analysis of the effect of the noise is presented in Section VI-B.

By referring to Fig. 3, the receiver derives an estimate $\hat{\alpha}_n$ with $n = 0, \dots, N - 1$ vectors using a low complex matched filter as

$$\hat{\alpha}_n = C_n^H s. \quad (18)$$

We can assume that $\hat{\alpha}_n = \alpha_n$ if C_n is correctly signaled and in case of an ideal transmission.

The n th transmitted waveform can be reconstructed at the receiver as

$$\hat{s}_n = C_n \hat{\alpha}_n. \quad (19)$$

At this point, the receiver follows the same procedure as the transmitter to derive the basis of the null space.

For the first antenna, $\hat{\alpha}_1$ is already informative, containing the symbols drawn from the given constellation. Then, by knowing \hat{s}_1 and C_1 , it is possible to derive \hat{W}_1 and from that the bases of the null space \hat{N}_1 . Once these bases are known, the information in β_2 can be decoded by simply performing a projection:

$$\hat{\beta}_2 = \hat{N}_1^H \hat{\alpha}_2. \quad (20)$$

In the same way, by knowing \hat{s}_1 , \hat{s}_2 and C_3 , the matrices \hat{W}_2 and \hat{W}_3 can be calculated and from those the matrix \hat{N}_2 . Once again, the information in β_3 can be estimated as:

$$\hat{\beta}_3 = \hat{N}_2^H \hat{\alpha}_3. \quad (21)$$

The process is performed sequentially up to the final transmitted signal, thus estimating all the informative β_n transmitted. A performance assessment of the communication system is presented in Section VI-B.

B. Imaging receiver

As depicted in Fig. 3, the imaging receiver is co-located with the transmitter and has the perfect knowledge of the set of signals \mathcal{S} . Each one of the M receiving antenna records the delayed echo of the coherent superposition of all the transmitted signals

$$\mathbf{s} = \sum_{n=1}^{n=N} \mathbf{s}_n. \quad (22)$$

The signals are separated at the receiver by a simple correlation or, in radar jargon, range compression

$$\tilde{\mathbf{S}}_n \mathbf{s} = \tilde{\mathbf{S}}_n (\mathbf{s}_1 + \mathbf{s}_2 + \dots + \mathbf{s}_N) = \tilde{\mathbf{S}}_n \mathbf{s}_n, \quad (23)$$

where the last equality holds due to the orthogonality between signals in (9) that can be generalized as

$$\tilde{\mathbf{S}}_n \mathbf{s}_m = \mathbf{0} \quad \forall \quad m \neq n. \quad (24)$$

The signal $\tilde{\mathbf{S}}_n \mathbf{s}_n$ is the auto-correlation of the n th signal calculated just within the zero correlation interval. Each receiving antenna performs the correlation with all the transmitting signals, leading to an equivalent number of virtual channels equal to $N \times M$. If TX and RX antenna elements are appropriately spaced, the elements of the generated monostatic virtual array will be spaced by $\lambda/4$, leading to the unambiguous imaging of the whole field of view [50]. An analysis of the imaging performances of the system is presented in Section VI-A

V. IMAGING AND COMMUNICATION EFFICIENCY

In this section, we analytically demonstrate that the efficiency of the sensing and communication sub-systems can be opportunely tuned, privileging the former or the latter. The tuning is performed by allocating the number of waveforms that transmit information or by selecting the number of communication symbols for each transmission.

The system is flexible, and many different configurations can be implemented. We can define the communication efficiency as the ratio between the decoded communication symbols and the pulse length as

$$\eta_{\text{comm}} = \frac{N_{\text{sym}}}{K}. \quad (25)$$

The efficiency of the sensing can be expressed as the ratio between the samples at zero correlation and the total length of the waveform

$$\eta_{\text{sens}} = \frac{K_z}{K} < \frac{1}{N-1}. \quad (26)$$

Interestingly, it is possible to reach a unitary sensing efficiency with two antennas where the two waveforms will be orthogonal for their entire length ($K_z = K$).

In a sensing-favored scenario, only a single waveform encodes information, and all the others are used for sensing operations, leading to a different model of the received signal

$$\mathbf{s} = \mathbf{C}_1 \boldsymbol{\alpha}_1 + \mathbf{C}_2 (\boldsymbol{\alpha}_2 + \boldsymbol{\alpha}_3 + \dots + \boldsymbol{\alpha}_N). \quad (27)$$

In this scenario, only the information into $\boldsymbol{\alpha}_1$ can be decoded at the receiver. All the others are even if \mathbf{C}_2^H is used as a matched filter. Notice that the sizes of \mathbf{C}_1 and \mathbf{C}_2 can be

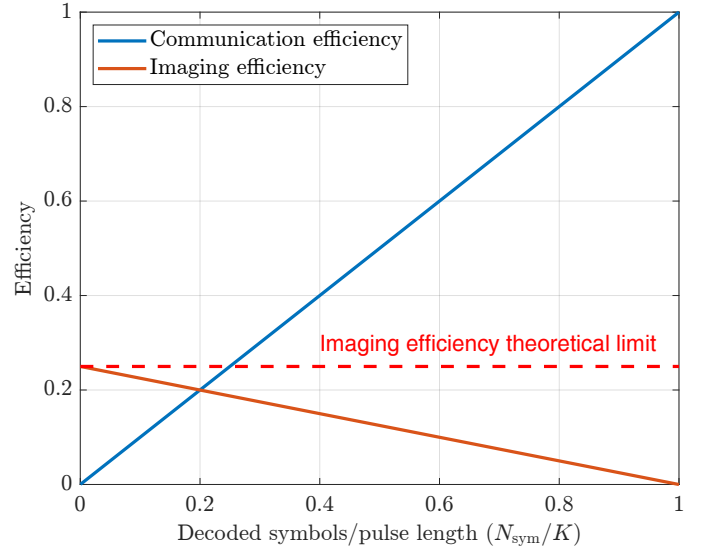


Fig. 7: Communication and sensing efficiency using 5 antennas and only the first one dedicated to imaging and communication. All the others are dedicated only to imaging.

designed to give more efficiency to the sensing system and less to the communication system or vice versa.

In case of transmission with only imaging purposes, the n th waveform can be designed as

$$\mathbf{s}_n = \mathbf{C}_1 \boldsymbol{\alpha}_n, \quad (28)$$

where it is essential to notice that the key \mathbf{C}_1 is fixed for all the signals and coincides with the entire master key \mathbf{C} . At the receiver, the recorded signal will be a delayed version of

$$\begin{aligned} \mathbf{s} &= \mathbf{C}_1 \boldsymbol{\alpha}_1 + \mathbf{C}_1 \boldsymbol{\alpha}_2 + \dots + \mathbf{C}_1 \boldsymbol{\alpha}_N \\ &= \mathbf{C}_1 (\boldsymbol{\alpha}_1 + \boldsymbol{\alpha}_2 + \dots + \boldsymbol{\alpha}_N). \end{aligned} \quad (29)$$

Intuitively, it is not possible to recover the vectors $\boldsymbol{\alpha}_n$.

In the case of a communication-favored system, the amount of information is transmitted without requiring waveform orthogonality. Thus, no imaging can occur. In the case of $\eta_{\text{comm}} = 1$, a number of symbols equal to the pulse length ($N_{\text{sym}} = K$) is transmitted. It is possible to assign to each antenna the same signal

$$\mathbf{s}_n = \mathbf{C}_1 \boldsymbol{\alpha}_1, \quad (30)$$

where $\boldsymbol{\alpha}_1$ contains K constellation symbols. At the receiver, the recorded signal will be a delayed version of

$$\begin{aligned} \mathbf{s} &= \mathbf{C}_1 \boldsymbol{\alpha}_1 + \mathbf{C}_1 \boldsymbol{\alpha}_1 + \dots + \mathbf{C}_1 \boldsymbol{\alpha}_1 \\ &= N \mathbf{C}_1 \boldsymbol{\alpha}_1. \end{aligned} \quad (31)$$

Notably, a gain by factor of N resembles the one obtainable from the beamforming techniques, wherein phase shifting of the signal $\boldsymbol{\alpha}_1$ can be employed across each antenna to focus transmission signals in specific directions using antenna arrays. This improves signal strength by directing energy towards targeted users or areas. The K symbols can be estimated using a matched filter $\hat{\boldsymbol{\alpha}}_1 = \mathbf{C}_1^H \mathbf{s}$. However, there will be no orthogonality at all between the signals. To generalize, we

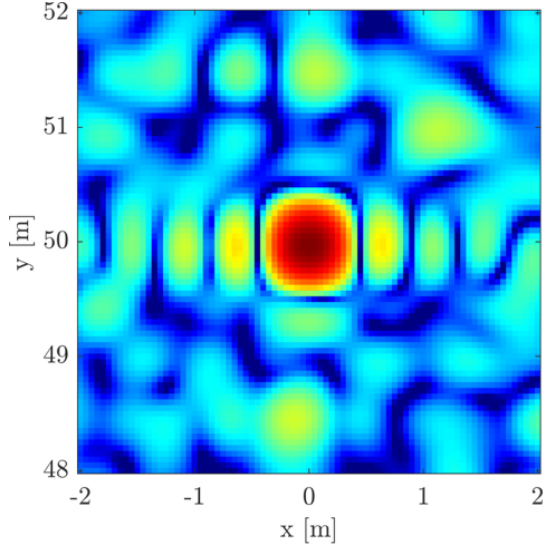


Fig. 8: Image of the scene generated using waveforms respecting the orthogonality condition in Appendix A. The noise floor is high, and faint targets are hidden by MIMO noise.

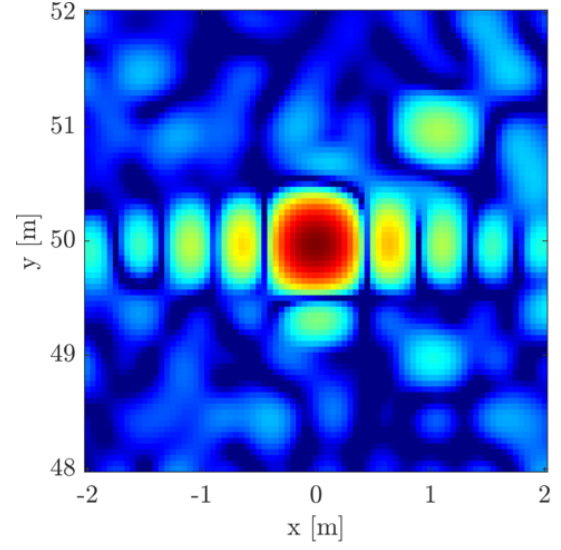


Fig. 9: Image of the scene generated using COSMIC waveforms. The MIMO noise is much lower, and detecting faint targets is now possible thanks to a lower noise floor.

consider the case of N_b different key matrices as

$$\mathbf{s} = \mathbf{C}_1 \boldsymbol{\alpha}_1 + \mathbf{C}_2 \boldsymbol{\alpha}_2 + \dots + \mathbf{C}_{N_b} (\dots + \boldsymbol{\alpha}_N), \quad (32)$$

where $\boldsymbol{\alpha}_n$ are informative for $n = 1, \dots, N_b - 1$. By calling K_s^n the number of columns of the matrix \mathbf{C}_n , the following constraints can be considered

$$K_z(N-1) < K_s^{N_b} \rightarrow K_z(N-1) = K_s^{N_b} - 1 \quad (33)$$

$$\sum_{n=1}^{N_b} K_s^n = K. \quad (34)$$

In Fig. 7, the efficiency of communication and sensing are shown for varying N_{sym}/K with $N = 5$ and $N_b = 2$. In this case, to ensure N_{sym} transmitted symbols, we have to set $K_s^1 = N_{\text{sym}}$ and $K_s^2 = K - N_{\text{sym}}$. Equation (33) can be written as

$$K_z(N-1) = K_s^{N_b} - 1 = K - N_{\text{sym}} - 1, \quad (35)$$

thus, the sensing efficiency η_{sens} is

$$\eta_{\text{sens}} = \frac{K_z}{K} = \frac{K - N - 1}{K(N-1)}. \quad (36)$$

VI. NUMERICAL RESULTS

This section presents the numerical results of the proposed COSMIC waveforms for both the communication and imaging receivers.

A. Imaging performances

We consider realistic scenarios where a target with a small Radar Cross-Section (RCS) is located next to a target with a larger one. This is typical in an automotive scenario in which, for example, a pedestrian is standing close to a vehicle. In our simulations, 15 antennas simultaneously illuminate the scene, and 15 antennas receive the echo back from the scene. The

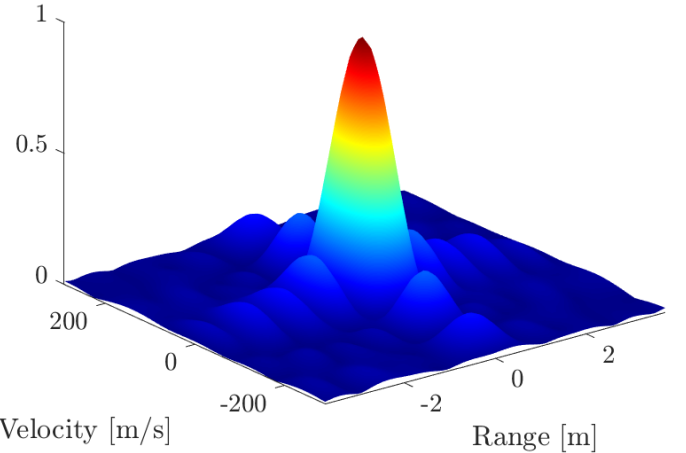


Fig. 10: Range/Velocity ambiguity function of a COSMIC waveform. The bandwidth is set to 200 MHz, leading to a range resolution of 0.75m. The pulse length is 20 μs , leading to a ≈ 100 m/s velocity resolution.

TX and RX elements are located in such a way as to form a monostatic Uniform Virtual Array (ULA) of 225 elements spaced by $\lambda/4$. After range compression, the image is formed using Time Domain Back Projection (TDBP) [51]. In Fig. 8, the formed image is shown in the case where the transmitted waveforms respect only the orthogonality condition defined in (3). As shown in Fig. 2, the noise floor due to MIMO noise is very high, faint targets are difficult to detect, and false alarms could be a serious concern. On the other hand, in Fig. 9, the same scenario is focused using COSMIC waveforms respecting the orthogonality condition in 4. The MIMO noise floor is much lower than the previous case, allowing for the detection of the faint target located at $x = 1$ m and $y = 51$ m. As expected, the Impulse Response Function (IRF) is close to a bi-dimensional cardinal sine, and the size of the main lobe is

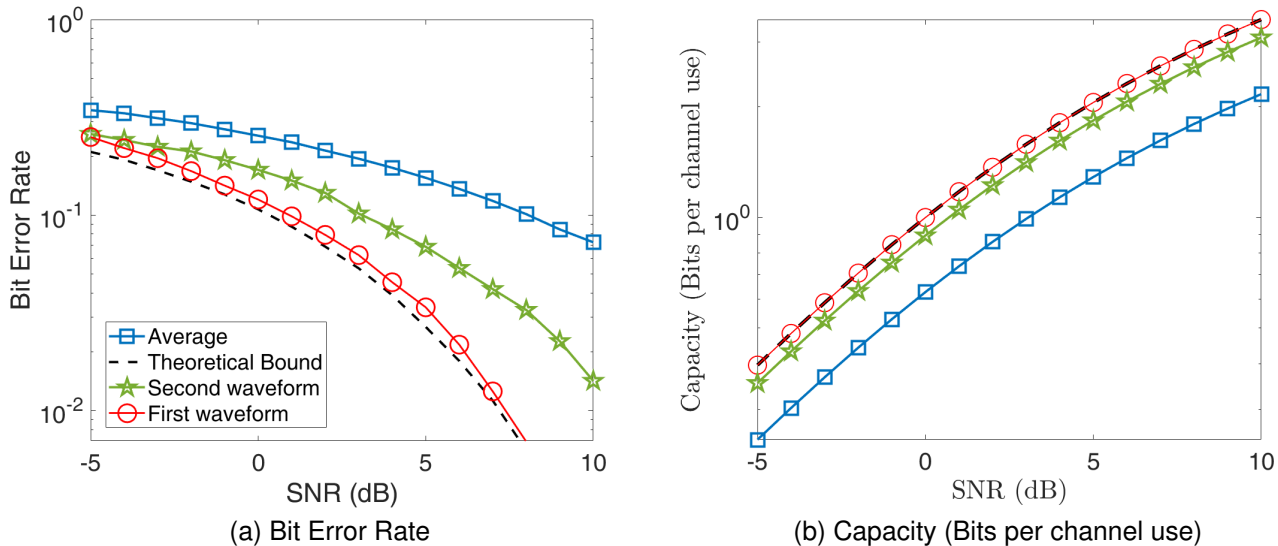


Fig. 11: 16-QAM a) Bit Error Rate and b) Capacity versus Signal-to-Noise Ratio by considering the first and second transmitted waveforms only and the average overall the $N = 8$ transmitted ones.

inversely proportional to the bandwidth and the aperture size. In Fig. 10, a COSMIC waveform’s range/velocity ambiguity function is depicted. As expected by the pseudo-random nature of the waveform, the ambiguity function shows a bi-sinc-like behavior, meaning that range and velocities are not ambiguous, unlike other standard waveforms in radar imaging (i.e., chirp functions).

B. Communication performances

The COSMIC performance at the communication receiver is evaluated using the Bit-Error-Rate (BER) and the system capacity (in bits per channel use) of a 16 QAM modulation for different Signal-to-Noise Ratio (SNR) values in dB. The simulations consider a Multi-Input-Single-Output (MISO), where the RadCom has $N = 8$ antennas. The COSMIC performance is compared with the theoretical one. The performance for the symbols transmitted only by the first two waveforms, as well as the average across all antennas, is reported.

As shown in Fig. 11a, the BER for the first waveform is close to the theoretical value and coincides with the ideal receiver case. However, since the \hat{s}_1 differs from s_1 due to the presence of noise in the estimation of the null spaces, an error propagation is present. Consequently, the performance degrades for the symbols transmitted by the second waveforms. This results in an average BER across all the waveforms, which is sequentially and increasingly affected by this error propagation, and consequently, gets worse. It is worth stating that such an errors propagation can be mitigated by applying power and bit loading algorithms and/or a non linear dirty paper-like coding approaches at the RadCom or soft iterative detection algorithms at the communication receiver [52].

Figure 11b presents the COSMIC capacity in bits per channel use in comparison to the Shannon formula. The results for the first waveform coincides with the theoretical bound. A

minor degradation is observed for the sequence transmitted to the second antenna due to lower communication efficiency as explained in Sec. V and the interference generated by incorrect estimation of the null space at the receiver, as previously explained. When averaging the capacity across all waveforms, this effect slightly reduces the overall COSMIC capacity.

VII. CONCLUSIONS

This paper has introduced COSMIC (Connectivity-Oriented Sensing Method for Imaging and Communication), a novel waveform design method that effectively integrates the functionalities of radar imaging and communication within the same system. The main innovation of COSMIC waveforms lies in their ability to convey communication symbols while satisfying an extended orthogonality condition, facilitating their dual use in generating radio images of the environment. Through the implementation of a MIMO Radar-Communication (RadCom) device, COSMIC waveforms are transmitted from multiple antennas simultaneously within the same time window and frequency band, demonstrating that the orthogonality of these waveforms is not dependent on time or frequency separation. Instead, it is achieved by leveraging the degrees of freedom offered by the assumption that the field of view is limited or significantly smaller than the length of the transmitted signals.

The paper details the iterative processing procedure used to generate the waveforms. The workflow employed on the receiver side is also described in detail, and the efficiency of both the imaging and communication sub-systems is discussed. The efficiency can be tuned arbitrarily, prioritizing the former or the latter depending on the scenario, the amount of information to be transmitted, and the desired imaging resolution. The system’s performance is assessed, demonstrating its capability to image and detect faint targets, thanks to the complete

absence of MIMO noise. At the same time, the BER of the communication is evaluated, showing that for the first antenna, the BER coincides with the ideal one. In contrast, there is a forwarding error for increasing antenna index, which leads to a degradation of the performances.

APPENDIX A

ORTHOGONALITY FOR PERFECT SIGNAL SEPARATION

Let us suppose to have an extended scattering scenario with N_p targets illuminated by N waveforms. The signal received by a generic antenna is a delayed version of the superposition of all the transmitted signals.

$$s_{\text{rx}}(t) = \sum_{p=1}^{N_p} s_{\text{tx}}(t - \tau_p). \quad (37)$$

where $s_{\text{tx}}(t) = s_1(t) + s_2(t) + \dots + s_N(t)$ and τ_p is the two-way travel time from the transmitter to the target and from the target to the receiver. Equation (37) omits all the amplitude factors related to the propagation losses and the target's Radar Cross Section (RCS). Using a matched filter, the receiver must be able to separate the contribution from each antenna. To separate the contribution of the first antenna, we cross-correlate the received signal with $s_1(t)$ as

$$s_{\text{rx}}(t) * s_1^*(-t) = \int_{-\infty}^{+\infty} \sum_{p=1}^{N_p} s_{\text{tx}}(\eta + t - \tau_p) s_1^*(\eta) d\eta. \quad (38)$$

To address the interference effect between waveforms, we fix a generic target (for example, the first one) and compute (38) for $t = \tau_1$. Such that

$$s_{\text{rx}}(t) * s_1^*(-t)|_{t=\tau_1} = \sum_{n=1}^N r_{1n}(0) + \quad (39)$$

$$+ \sum_{p=2}^{N_p} \int_{-\infty}^{+\infty} s_1(\eta + \Delta\tau_{1p}) s_1^*(\eta) d\eta \quad (40)$$

$$+ \sum_{p=2}^{N_p} \sum_{n=2}^N \int_{-\infty}^{+\infty} s_n(\eta + \Delta\tau_{1p}) s_1^*(\eta) d\eta, \quad (41)$$

where $r_{1n}(0)$ is the value of the peak of the cross-correlation between the first signal and the n^{th} one and $\Delta\tau_{1p} = \tau_1 - \tau_p$. Different simplifications are possible depending on the degree of orthogonality between the waveforms. If the waveforms are orthogonal as in (3), the term in (39) simplifies, and only the auto-correlation of $s_1(t)$ remains:

$$\sum_{n=1}^N r_{1n}(0) = r_{11}(0). \quad (42)$$

However, notice how the condition in (3) is insufficient to suppress the interference among waveforms in the case of an extended scattering scenario. In fact, (41) represents the so-called *MIMO noise*, whose power grows with the number of targets in the scene and the number of transmitting antennas. The only way to completely suppress this term is to guarantee zero cross-correlation between the waveforms for any arbitrary

shift or, for scenes with limited size, for any possible $\Delta\tau_{1p}$ (as in (4)). Finally, (40) represents the sidelobes of the auto-correlation of $s_1(t)$ associated with all the targets in the scene, leaking over the target under consideration. This term is negligible for $\Delta\tau_{1p}$ much larger than the resolution ($\approx 1/B$, where B is the bandwidth).

REFERENCES

- [1] F. Dong, F. Liu, Y. Cui, S. Lu, and Y. Li, "Sensing as a service in 6g perceptive mobile networks: Architecture, advances, and the road ahead," *IEEE Network*, pp. 1–1, 2024.
- [2] U. Demirhan and A. Alkhateeb, "Integrated sensing and communication for 6g: Ten key machine learning roles," *IEEE Communications Magazine*, 2023.
- [3] A. Kaushik, R. Singh, S. Dayarathna, R. Senanayake, M. Di Renzo, M. Dajer, H. Ji, Y. Kim, V. Sciancalepore, A. Zappone, and W. Shin, "Toward integrated sensing and communications for 6g: Key enabling technologies, standardization, and challenges," *IEEE Communications Standards Magazine*, vol. 8, no. 2, pp. 52–59, 2024.
- [4] A. Wilson-Langman, M. R. Inggs, and A. K. Mishra, "Symbiotic radar and communication system," Sep. 25 2018, uS Patent 10,082,561.
- [5] T. M. Kellum, W. B. SCHULTE, H. B. Marr *et al.*, "System and method for concurrent communication of different signal types by a radar," Mar. 24 2020, uS Patent 10,598,763.
- [6] C. Davis, M. Hegde, W. E. Stark, A. Eshraghi, M. Goldenberg, and M. Ali, "Vehicle radar system with a shared radar and communication system," Jan. 14 2020, uS Patent 10,536,529.
- [7] J. A. Zhang, F. Liu, C. Masouros, R. W. Heath, Z. Feng, L. Zheng, and A. Petropulu, "An overview of signal processing techniques for joint communication and radar sensing," *IEEE Journal of Selected Topics in Signal Processing*, vol. 15, no. 6, pp. 1295–1315, 2021.
- [8] A. Zhang, M. L. Rahman, X. Huang, Y. J. Guo, S. Chen, and R. W. Heath, "Perceptive mobile networks: Cellular networks with radio vision via joint communication and radar sensing," *IEEE Vehicular Technology Magazine*, vol. 16, no. 2, pp. 20–30, 2021.
- [9] Y. Liu, G. Liao, Z. Yang, and J. Xu, "Design of integrated radar and communication system based on mimo-ofdm waveform," *Journal of Systems Engineering and Electronics*, vol. 28, no. 4, pp. 669–680, 2017.
- [10] A. Ali, N. Gonzalez-Prelcic, R. W. Heath, and A. Ghosh, "Leveraging sensing at the infrastructure for mmwave communication," *IEEE Communications Magazine*, vol. 58, no. 7, pp. 84–89, 2020.
- [11] G. Krieger, "MIMO-SAR: Opportunities and Pitfalls," *IEEE Transactions on Geoscience and Remote Sensing*, vol. 52, no. 5, pp. 2628–2645, May 2014. [Online]. Available: <https://ieeexplore.ieee.org/document/6549108/>
- [12] A. Hassanien, M. G. Amin, Y. D. Zhang, and F. Ahmad, "Signaling strategies for dual-function radar communications: An overview," *IEEE Aerospace and Electronic Systems Magazine*, vol. 31, no. 10, pp. 36–45, 2016.
- [13] S. D. Blunt, M. R. Cook, and J. Stiles, "Embedding information into radar emissions via waveform implementation," in *2010 International waveform diversity and design conference*. IEEE, 2010, pp. 000 195–000 199.
- [14] M. Jamil, H.-J. Zepernick, and M. I. Pettersson, "On integrated radar and communication systems using oppermann sequences," in *MILCOM 2008 - 2008 IEEE Military Communications Conference*, 2008, pp. 1–6.
- [15] S. Doğan Tusha, A. Tusha, E. Basar, and H. Arslan, "Multidimensional index modulation for 5g and beyond wireless networks," *Proceedings of the IEEE*, vol. 109, no. 2, pp. 170–199, 2021.
- [16] Z. Xu, A. Petropulu, and S. Sun, "A joint design of mimo-ofdm dual-function radar communication system using generalized spatial modulation," in *2020 IEEE Radar Conference (RadarConf20)*, 2020, pp. 1–6.
- [17] D. Ma, N. Shlezinger, T. Huang, Y. Liu, and Y. C. Eldar, "Joint radar-communication strategies for autonomous vehicles: Combining two key automotive technologies," *IEEE Signal Processing Magazine*, vol. 37, no. 4, pp. 85–97, 2020.
- [18] A. Hassanien, M. G. Amin, E. Aboutanios, and B. Himed, "Dual-function radar communication systems: A solution to the spectrum congestion problem," *IEEE Signal Processing Magazine*, vol. 36, no. 5, pp. 115–126, 2019.

- [19] M. Nowak, M. Wicks, Z. Zhang, and Z. Wu, "Co-designed radar-communication using linear frequency modulation waveform," *IEEE Aerospace and Electronic Systems Magazine*, vol. 31, no. 10, pp. 28–35, 2016.
- [20] F. Zhang, T. Mao, and Z. Wang, "Doppler-resilient design of cazac sequences for mmwave/thz sensing applications," *arXiv preprint arXiv:2305.07234*, 2023.
- [21] P. Yuan, Z. Wang, Q. Huang, and Y. Ni, "Integrated sensing and communications system with multiple cyclic prefixes," *IEEE Communications Letters*, vol. 27, no. 8, pp. 2043–2047, 2023.
- [22] S. Aditya, O. Dizdar, B. Clerckx, and X. Li, "Sensing using coded communications signals," *IEEE Open Journal of the Communications Society*, vol. 4, pp. 134–152, 2022.
- [23] Y. Zeng, Y. Ma, and S. Sun, "Joint radar-communication with cyclic prefixed single carrier waveforms," *IEEE Transactions on Vehicular Technology*, vol. 69, no. 4, pp. 4069–4079, 2020.
- [24] C. Sturm and W. Wiesbeck, "Waveform design and signal processing aspects for fusion of wireless communications and radar sensing," *Proceedings of the IEEE*, vol. 99, no. 7, pp. 1236–1259, 2011.
- [25] L. Pucci, E. Paolini, and A. Giorgetti, "System-level analysis of joint sensing and communication based on 5G New Radio," *IEEE J. Sel. Areas Commun.*, 2022, to appear.
- [26] L. Pucci, E. Matricardi, E. Paolini, W. Xu, and A. Giorgetti, "Performance analysis of joint sensing and communication based on 5G New Radio," in *2021 IEEE Globecom Workshops (GC Wkshps)*, Dec. 2021, pp. 1–6.
- [27] Y. Liu, G. Liao, Y. Chen, J. Xu, and Y. Yin, "Super-resolution range and velocity estimations with ofdm integrated radar and communications waveform," *IEEE Transactions on Vehicular Technology*, vol. 69, no. 10, pp. 11 659–11 672, 2020.
- [28] C. Shi, F. Wang, M. Sellathurai, J. Zhou, and S. Salous, "Power minimization-based robust ofdm radar waveform design for radar and communication systems in coexistence," *IEEE Transactions on Signal Processing*, vol. 66, no. 5, pp. 1316–1330, 2018.
- [29] N. Bekkali, M. Benammar, S. Bidon, and D. Roque, "Optimal power allocation in monostatic ofdm joint radar communications systems," in *2022 IEEE Radar Conference (RadarConf22)*, 2022, pp. 1–6.
- [30] Y. Zhang, S. Aditya, and B. Clerckx, "Input distribution optimization in ofdm dual-function radar-communication systems," 2023.
- [31] Y. Liu, G. Liao, J. Xu, Z. Yang, and Y. Zhang, "Adaptive ofdm integrated radar and communications waveform design based on information theory," *IEEE Communications Letters*, vol. 21, no. 10, pp. 2174–2177, 2017.
- [32] Z. Du, Z. Zhang, and W. Yu, "Information theoretic waveform design for ofdm radar-communication coexistence in gaussian mixture interference," *IET Radar, Sonar & Navigation*, vol. 13, no. 11, pp. 2063–2070, 2019. [Online]. Available: <https://ietresearch.onlinelibrary.wiley.com/doi/abs/10.1049/iet-rsn.2019.0276>
- [33] M. Bica, K.-W. Huang, U. Mitra, and V. Koivunen, "Opportunistic radar waveform design in joint radar and cellular communication systems," in *2015 IEEE Global Communications Conference (GLOBECOM)*, 2015, pp. 1–7.
- [34] M. Bičá and V. Koivunen, "Multicarrier radar-communications waveform design for rf convergence and coexistence," in *ICASSP 2019 - 2019 IEEE International Conference on Acoustics, Speech and Signal Processing (ICASSP)*, 2019, pp. 7780–7784.
- [35] C. Baquero Barneto, T. Riihonen, M. Turunen, L. Anttila, M. Fleischer, K. Stadius, J. Ryyänen, and M. Valkama, "Full-duplex ofdm radar with lte and 5g nr waveforms: Challenges, solutions, and measurements," *IEEE Transactions on Microwave Theory and Techniques*, vol. 67, no. 10, pp. 4042–4054, 2019.
- [36] S. D. Liyanaarachchi, T. Riihonen, C. B. Barneto, and M. Valkama, "Optimized waveforms for 5g–6g communication with sensing: Theory, simulations and experiments," *IEEE Transactions on Wireless Communications*, pp. 1–1, 2021.
- [37] E. Memisoglu, T. Yilmaz, and H. Arslan, "Waveform Design with Constellation Extension for OFDM Dual-Functional Radar-Communications," 11 2022.
- [38] P. Kumari, S. A. Vorobyov, and R. W. Heath, "Adaptive virtual waveform design for millimeter-wave joint communication–radar," *IEEE Transactions on Signal Processing*, vol. 68, pp. 715–730, 2020.
- [39] M. F. Keskin, V. Koivunen, and H. Wymeersch, "Limited feedforward waveform design for ofdm dual-functional radar-communications," *IEEE Transactions on Signal Processing*, vol. 69, pp. 2955–2970, 2021.
- [40] P. Raviteja, K. T. Phan, Y. Hong, and E. Viterbo, "Orthogonal time frequency space (otfs) modulation based radar system," in *2019 IEEE Radar Conference (RadarConf)*, 2019, pp. 1–6.
- [41] L. Gaudio, M. Kobayashi, G. Caire, and G. Colavolpe, "On the effectiveness of ofts for joint radar parameter estimation and communication," *IEEE Transactions on Wireless Communications*, vol. 19, no. 9, pp. 5951–5965, 2020.
- [42] L. Gaudio, M. Kobayashi, B. Bissinger, and G. Caire, "Performance analysis of joint radar and communication using ofdm and ofts," in *2019 IEEE International Conference on Communications Workshops (ICC Workshops)*. IEEE, 2019, pp. 1–6.
- [43] D. Tagliaferri, M. Mizmizi, S. Mura, F. Linsalata, D. Scazzoli, D. Badini, M. Magarini, and U. Spagnolini, "Integrated sensing and communication system via dual-domain waveform superposition," *IEEE Transactions on Wireless Communications*, 2023.
- [44] F. Zhang, T. Mao, R. Liu, H. Zhu, S. Chen, and Z. Wang, "Cross-domain dual-functional ofdm waveform design for accurate sensing/positioning," *IEEE Journal on Selected Areas of Communications*, 2024.
- [45] A. Bemani, N. Ksairi, and M. Kountouris, "Integrated sensing and communications with affine frequency division multiplexing," *arXiv preprint arXiv:2402.16468*, 2024.
- [46] S. Lu, F. Liu, F. Dong, Y. Xiong, J. Xu, Y.-F. Liu, and S. Jin, "Random isac signals deserve dedicated precoding," *arXiv preprint arXiv:2311.01822*, 2023.
- [47] B. Zheng and F. Liu, "Waveform design for joint communication and sar imaging under random signaling," *arXiv preprint arXiv:2403.17627*, 2024.
- [48] F. Liu, L. Zhou, C. Masouros, A. Li, W. Luo, and A. Petropulu, "Toward Dual-functional Radar-Communication Systems: Optimal Waveform Design," *IEEE Transactions on Signal Processing*, vol. 66, no. 16, pp. 4264–4279, Aug. 2018. [Online]. Available: <https://ieeexplore.ieee.org/document/8386661/>
- [49] S. Tebaldini, M. Rizzi, M. Manzoni, A. M. Guarnieri, C. Prati, D. Tagliaferri, M. Nicoli, U. Spagnolini, I. Russo, and C. Mazzucco, "SAR imaging in automotive scenarios," in *2022 Microwave Mediterranean Symposium (MMS)*. Pizzo Calabro, Italy: IEEE, May 2022, pp. 1–5. [Online]. Available: <https://ieeexplore.ieee.org/document/9825599/>
- [50] S. Tebaldini, M. Manzoni, D. Tagliaferri, M. Rizzi, A. V. Monti-Guarnieri, C. M. Prati, U. Spagnolini, M. Nicoli, I. Russo, and C. Mazzucco, "Sensing the Urban Environment by Automotive SAR Imaging: Potentials and Challenges," *Remote Sensing*, vol. 14, no. 15, p. 3602, Jan. 2022, number: 15 Publisher: Multidisciplinary Digital Publishing Institute. [Online]. Available: <https://www.mdpi.com/2072-4292/14/15/3602>
- [51] M. Manzoni, S. Tebaldini, A. V. Monti-Guarnieri, C. M. Prati, and I. Russo, "A Comparison of Processing Schemes for Automotive MIMO SAR Imaging," *Remote Sensing*, vol. 14, no. 19, p. 4696, Sep. 2022. [Online]. Available: <https://www.mdpi.com/2072-4292/14/19/4696>
- [52] K. Kusume, M. Joham, W. Utschick, and G. Bauch, "Efficient tomlinson-harashima precoding for spatial multiplexing on flat mimo channel," in *IEEE International Conference on Communications, 2005. ICC 2005*, 2005, vol. 3. IEEE, 2005, pp. 2021–2025.